

# Integrating discretization and association rule-based classification for Alzheimer's disease diagnosis

R. Chaves\*, J. Ramírez, J.M. Górriz for the Alzheimer's Disease Neuroimaging Initiative<sup>1</sup>

Dept. Signal Theory, Networking and Communication, ETSIT, 18071, University of Granada, Spain

## ARTICLE INFO

### Keywords:

Association rules  
Discretization  
Image histogram  
Alzheimer's disease  
Computed aided diagnosis

## ABSTRACT

This paper shows a computer aided diagnosis (CAD) combining continuous attribute discretization and association rule mining for the early diagnosis of Alzheimer's disease (AD) based on emission computed tomography images. A mask is obtained from the mean control images by an image histogram segmentation. 3D voxels centered in mask coordinates are selected by equal-width binning-based discretization of the mean intensity. These Regions of Interest (ROIs) are then used as input for the Association Rule (AR)-mining using control subject images to fully characterize the normal pattern of the image. Minimum support and confidence are fixed to the maximum values in order to obtain the highest predictive power rules for each discretization level (or combination of levels). Finally, classification is carried out by comparing the number of ARs verified by each subject under test. The proposed system is evaluated using two different databases of single photon emission computed tomography (SPECT) and positron emission tomography (PET) images from the Alzheimer Disease Neuroimaging Initiative (ADNI) yielding an accuracy up to 96.91% (for SPECT) and 92% (for PET), thus outperforming the baseline (the so called continuous AR-based method) and other recently reported CAD methods.

© 2012 Elsevier Ltd. All rights reserved.

## 1. Introduction

The number of people with Alzheimer's disease (AD) is expected to increase in the following decades, thus there is a need for finding solutions that not only delay but also prevent its development which is becoming an urgent public health concern. The current diagnostic process should be refocussed toward the pathological substrate of this disease rather than symptoms in order to initiate therapeutic measures as soon as possible without waiting for clinical manifestations to appear (Brookmeyer, Johnson, Ziegler-Graham, & Michael Arrighi, 2007).

Currently, AD diagnosis is based on the information provided by a careful clinical examination, in-depth interview of the patient and relatives, and a neuropsychological assessment. Along with those tests, nuclear medicine and magnetic resonance imaging have proven its efficiency as a non-invasive tool for diagnosis (Ng, Villemagne, & Berlangieri, 2007). Brain functional imaging, such as Single Photon Emission Computed Tomography (SPECT)

or Positron Emission Tomography (PET), have been proved to be a very effective tool for data extraction in the early diagnosis of AD by using non-invasive methods (Kogure et al., 2000). In this sense, SPECT provides functional information, i.e., regional cerebral blood flow (rCBF) for identifying pathologic anomalies in internal tissues or organs, even before anatomical and structural alterations are observable. On the other hand, PET measures the rate of glucose metabolism with the tracer <sup>18</sup>F-Fluorodeoxyglucose.

Computer Aided Diagnosis (CAD) tools based on medical imaging are a very valuable help for physicians in the AD detection (Chyzhyk, Graña, Savio, & Maiora, 2012; Segovia et al., 2012; Martínez-Murcia, Górriz, Ramírez b, Puntonet, & Salas-Gonzalez, 2012; Chaves et al., 2009). Whereas univariate CAD approaches process each voxel more or less independently (Friston, Ashburner, Kiebel, Nichols, & Penny, 2007b), multivariate approaches directly define functional connectivity across the brain by the analysis of regions of interest (ROIs) (López et al., 2009). In the latter case, the higher dimensionality of the input feature space in comparison with the relatively small number of subjects arises various problems such as curse of dimensionality and large hypothesis space, thus some form of feature selection is often required in order to discard some irrelevant and/or redundant features, that not only make learning harder, but also degrade generalization performance of statistical learning models. Several feature selection approaches have been proposed and can be broadly classified into three categories: the filter approach, the wrapper approach, and the hybrid approach

\* Corresponding author.

E-mail address: [rosach@ugr.es](mailto:rosach@ugr.es) (R. Chaves).

<sup>1</sup> Data used in preparation of this article were obtained from the Alzheimer's Disease Neuroimaging Initiative (ADNI) database ([adni.loni.ucla.edu](http://adni.loni.ucla.edu)). As such, the investigators within the ADNI contributed to the design and implementation of ADNI and/or provided data but did not participate in analysis or writing of this report. A complete listing of ADNI investigators can be found at: [http://adni.loni.ucla.edu/wp-content/uploads/how\\_to\\_apply/ADNI\\_Acknowledgement\\_List.pdf](http://adni.loni.ucla.edu/wp-content/uploads/how_to_apply/ADNI_Acknowledgement_List.pdf).

(Kabir, Islam, & Murase, 2010). The proposed algorithm combines in a single step, feature selection (Chaves, Ramrez, Górriz, & Puntonet, 2012) and discretization as in Ribeiro, Traina, Traina, and Azevedo-Marques (2008).

Our adaptation involves discretizing continuous attributes (mean 3D voxel intensity) into histogram bins and is also motivated by an equal width interval binning (Dougherty, Kohavi, & Mehran Sahami, 1995). Combined or independently considered discretized bins define the value that the feature must possess to be considered in the Association Rule (AR)-mining stage. Properly discretized data can simplify the process of learning and may improve the generalizability of the learned results (Kim & Han, 2000).

This paper shows a novel method for finding associations among discrete attributes of functional images by: (i) examining the differences and analogies between databases, and (ii) selecting better bins to remove irrelevant features for AD early diagnosis. Classification is performed using an AR-based approach outperforming the AR-baseline approach (Chaves et al., 2011) in which the whole feature histogram is used for AR-mining. In this sense, the latter method limits the number of activated ROIs under AR-mining analysis.

The paper is organised as follows. Section 2 shows an introduction to discretization methods. Section 3 provides Association Rules background information. The SPECT and PET databases used to evaluate the proposed method are described in Section 4. Section 5 shows a novel voxel selection method based on intensity histogram masking and discretization, together with AR mining and classification stages. Finally, the evaluation experiments are detailed and discussed in Section 6 and conclusions are drawn in Section 7.

## 2. Discretization methods

A very large proportion of real data sets include continuous variables, that is, measured at the interval or ratio level. The process of partitioning continuous variables into categories is usually termed discretization whose first goal is to find a set of cut points to partition the range into a small number of intervals that have good class coherence. In addition, feature discretization is closely related to dimensionality reduction (Park & Lee, 2009). The second goal is to minimize the number of intervals without significant loss of attribute mutual independence (Kotsiantis & Kanellopoulos, 2006). In Liu, Hsu, and Ma (1998), it is proposed the discretizing of continuous attributes based on the classification predetermined class target in order to integrate classification and AR mining. Generally, the discretization methods can be categorized as: supervised or unsupervised, direct or incremental and static or dynamic (Dougherty et al., 1995). While local methods produce partitions that are applied to localized regions of the instance space; global methods, such as binning, produce a mesh over the entire  $n$ -dimensional continuous space (Chmielewski & Grzymala-Busse, 1994). In contrast to unsupervised, supervised methods make use of the class labels in the discretization process. Whereas static methods, such as binning or entropy-based partitioning (Fayyad & Irani, 1993), perform one discretization pass of the data of each feature and determine the value of the maximum number of intervals ( $K$ ); dynamic methods conduct a search for all the features simultaneously in order to capture interdependencies in feature discretization. Equal width interval binning is an unsupervised method often applied as a means for producing nominal values from continuous ones and involves dividing the range of observed values of a continuous feature into  $K$  (selected by the user) equally sized bins (Dougherty et al., 1995). If a variable  $x$  is observed to have values bounded by  $x_{min}$  and  $x_{max}$ , then this method computes

the bin width as  $\alpha = \frac{x_{max} - x_{min}}{K}$  and constructs bin boundaries at  $x_{min} + i \cdot \alpha$  where  $i = 1, \dots, K - 1$ .

## 3. Association rules

The standard association-rule mining discovers correlations among items within transactions (Agrawal & Srikant, 1994). The prototypical example of utilizing AR mining is market basket analysis (Jukic & Nestorov, 2006). However, ARs are a promising alternative in medical image classification (Chaves et al., 2011). For example, in Dua, Singh, and Thompson (2009), ARs are derived between various texture components extracted from segments of a mammography dataset and classification is performed using a unique weighted AR-based classifier. Moreover, (Ribeiro et al., 2009) proposes the Image Diagnosis Enhancement through AR (IDEA) method in order to improve CAD systems. Nowadays, AR-based methods are often employed to suggest a second opinion to the radiologist or a preliminary diagnosis of a new image, in which discretization of continuous values before extraction has been recently introduced. Nonetheless, the application of ARs to early diagnosis of AD is still a challenge, i.e., Chaves et al. (2011), where the method process image features that consists of continuous attributes to mine ARs.

The well-known *Apriori* algorithm was firstly proposed in Agrawal and Srikant (1994). In this context, *A priori* works iteratively over ROIs in order to identify the frequent itemsets and to generate relationships (ARs) among brain areas (Chaves et al., 2011). A transaction  $t$  is defined as an implication of the form “subject that contains activated  $X$  area is likely to contain an activated  $Y$  area as well” and is noted as  $X \Rightarrow Y$ , where  $X$  and  $Y$  belong to the set of transaction items (Jukic & Nestorov, 2006), or discretized ROIs in this work  $I = \{i_1, i_2, \dots, i_m\}$ . The *relevance* of each rule is measured by the *support* and *confidence* of the transaction. The *support* measures the proportion of transactions in the data set which contain the itemset, thus we are interested in rules with relatively high *support*. The *confidence* measures the strength of the correlation, thus rules with low confidence are not meaningful, even if their *support* is considerably high. To perform a search, the user has to specify a minimum support (*minsupp*) and a minimum confidence (*minconf*) for analyzing frequent itemsets (He, Xiong, Yang, & Park, 2011; Dasseni, Verykios, Elmagarmid, & Bertino, 2001).

## 4. Materials

### 4.1. ECD-SPECT database

SPECT images used in this work were acquired by means of a PRISM 3000 gammacamera after injecting a gamma emitting technetium-99 m labeled ethyl cysteinate dimer ( $^{99m}\text{Tc}$ -ECD) to each subject. These images were reconstructed from projection data by filtered backprojection (FBP) in combination with a Butterworth noise filter. Then, SPECT images were spatially normalized (Salas-Gonzalez, Górriz, Ramírez, Lassi, & Puntonet, 2008) in order to ensure that a given voxel in different images refer to the same anatomical position. This process was done by using Statistical Parametric Mapping (SPM) (Friston, Ashburner, Kiebel, Nichols, & Penny, 2007a) yielding  $69 \times 95 \times 79$  normalized SPECT images.

A direct comparison of the voxel intensities of the images of different subject is not possible without normalization of the intensities. Intensity level of the images is normalized to the maximum intensity, which is computed for each image individually by averaging over the 0.1% of the highest voxel intensities as in López et al. (2009).

The database is built up of imaging studies of subjects following the protocol of an hospital-based service. First, the neurologist

**Table 1**

Demographic details of the SPECT database. AD 1 = mild perfusion deficit, AD 2 = moderate deficit, AD 3 = severe deficit.  $\mu$  and  $\sigma$  stands for population mean and standard deviation, respectively.

	Num. of samples	Sex (M/F) (%)	Age $\mu$ [range/ $\sigma$ ]
CTRL	41	32.95/12.19	71.51 [46–85/7.99]
AD 1	30	10.97/18.29	65.20 [23–81/13.36]
AD 2	22	13.41/9.76	65.73 [46–86/8.25]
AD 3	4	0/2.43	76 [69–83/9.90]

**Table 2**

Demographic details of the PET dataset.  $\mu$  and  $\sigma$  stands for population mean and standard deviation respectively.

Demographic details			
	Num. of samples	Sex (M/F) (%)	Age $\mu$ [range/ $\sigma$ ]
CTRL	75	29.33/20.67	75.97 [62–86/4.91]
AD	75	31.33/18.67	75.72 [55–88/7.40]

evaluated the cognitive function, and those patients with findings of memory loss or dementia were referred to the nuclear medicine department in the *Virgen de las Nieves* hospital (Granada, Spain), in order to acquire complementary screening information for diagnosis.<sup>2</sup> Experienced physicians evaluated the images visually. The images were assessed using four different labels: Control (CTRL) for subjects without scintigraphic abnormalities and mild perfusion deficit (AD1), moderate deficit (AD2) and severe deficit (AD3), to distinguish between different levels of presence of hypo-perfusion patterns compatible with AD. In total, the database consists of  $N = 97$  subjects: 41 CTRL, 30 AD1, 22 AD2 and 4 AD3 (see Table 1 for demographic details). Since the patients are not pathologically confirmed, the subject's labels possess some degree of uncertainty, as the pattern of hypo-perfusion may not reflect the underlying pathology of AD, nor the different classification of scans necessarily reflect the severity of the patients symptoms. However, when pathological information is available, visual assessments by experts have been shown to be very sensitive and specific labeling methods, in contrast to neuropsychological tests Jobst, Barnettson, and Shepstone (1998), Dubois et al. (2007). Given that this is an inherent limitation of 'in vivo' studies, our working-assumption is that the labels are true, considering the subject label positive when belonging to any of the AD classes, and negative otherwise. This work does not imply any experimental intervention and has been performed under the approval and supervision of the Clinical and Investigation Ethical Commission of the University Hospital Virgen de las Nieves (CEIC).

#### 4.2. PET database

PET data was obtained from the ADNI Laboratory on NeuroImaging (LONI, University of California, Los Angeles) website (<http://www.loni.ucla.edu/ADNI/>). The ADNI was launched in 2003 by the National Institute on Aging (NIA), the National Institute of Biomedical Imaging and Bioengineering (NIBIB), the Food and Drug Administration (FDA), private pharmaceutical companies and non-profit organizations, as a 60 million, 5-year public-private partnership. The primary goal of ADNI has been to test whether serial magnetic resonance imaging (MRI), PET, other biological markers, and clinical and neuropsychological assessment can be

combined to measure the progression of mild cognitive impairment (MCI) and early AD. Determination of sensitive and specific markers of very early AD progression is intended to aid researchers and clinicians to develop new treatments and monitor their effectiveness, as well as lessen the time and cost of clinical trials. The Principal Investigator of this initiative is Michael W. Weiner, MD, VA Medical Center and University of California – San Francisco. ADNI is the result of efforts of many co-investigators from a broad range of academic institutions and private corporations, and subjects have been recruited from over 50 sites across the US and Canada. The initial goal of ADNI was to recruit 800 adults, ages 55–90, to participate in the research, approximately 200 cognitively normal older individuals to be followed for 3 years, 400 people with MCI to be followed for 3 years and 200 people with early AD to be followed for 2 years. For up-to-date information, see [www.adni-info.org](http://www.adni-info.org). FDG PET scans were acquired according to a standardized protocol. A 30-min dynamic emission scan, consisting of 6 5-min frames, was acquired starting 30 min after the intravenous injection of  $5.0 \pm 0.5$  mCi of  $^{18}\text{F}$ -FDG, as the subjects, who were instructed to fast for at least 4 h prior to the scan, lay quietly in a dimly lit room with their eyes open and minimal sensory stimulation. Data were corrected for radiation-attenuation and scatter using transmission scans from Ge-68 rotating rod sources and reconstructed using measured-attenuation correction and image reconstruction algorithms specified for each scanner. Following the scan, each image was reviewed for possible artifacts at the University of Michigan and all raw and processed study data was archived. Subsequently, the images were normalized through a general affine model, with 12 parameters (Salas-Gonzalez et al., 2008) using the SPM5 software. After the affine normalization, the resulting image was registered using a more complex non-rigid spatial transformation model. The non-linear deformations to the Montreal Neurological Imaging (MNI) Template were parameterized by a linear combination of the lowest-frequency components of the three-dimensional cosine transform bases (Ashburner & Friston, 1999). A small-deformation approach was used, and regularization was by the bending energy of the displacement field, ensuring that the voxels in different FDG-PET images refer to the same anatomical positions in the brains. After spatial normalization, an intensity normalization was required in order to perform direct images comparisons between different subjects. The intensity of the images was normalized to a value  $I_{max}$ , obtained averaging the 0.1% of the highest voxel intensities exceeding a threshold. The threshold was fixed to the 10th bin intensity value of a 50-bins intensity histogram, for discarding most low intensity records from outside-brain regions, and preventing image saturation. Participant's enrolment was conditioned to some eligibility criteria. General inclusion–exclusion criteria were as follows:

- Normal control subjects: Mini Mental State Examination (MMSE) scores between 24 and 30 (inclusive), a Clinical Dementia Ratio (CDR) of 0, non depressed, non MCI, and non demented. The age range of normal subjects will be roughly matched to that of MCI and AD subjects. Therefore, there should be minimal enrolment of normals under the age of 70.
- Mild AD: MMSE scores between 20 and 26 (inclusive), CDR of 0.5 or 1.0, and meets NINCDS/ADRDA criteria for probable AD.

The PET database collected from ADNI consists of 150 labeled PET images: 75 control subjects and 75 AD patients (see Table 2 for demographic details). ADNI patient diagnostics are not pathologically confirmed, introducing some uncertainty on the subject's labels. Using these labels, allows to test the robustness of the classifier. This should be also considered when comparing to other methods tested on autopsy confirmed AD patients, on which every classifier is expected to improve its performance (Illán et al., 2011).

<sup>2</sup> Clinical information is unfortunately not available for privacy reasons, but only demographic information.

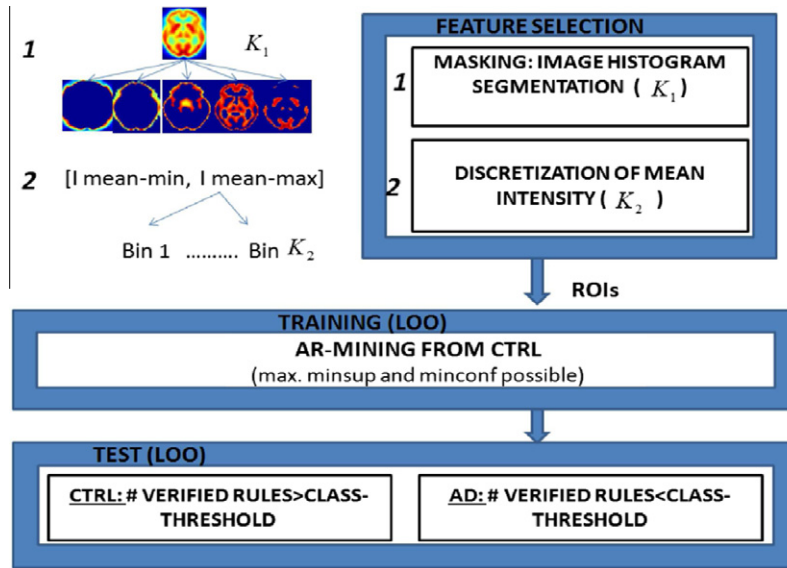


Fig. 1. Pipeline with the stages of the proposed CAD system: feature selection, training and test.

5. Description and methodology of the CAD system

In this section, the operation of the complete CAD system operation is described in detail, from image histogram for the masking procedure followed by discretization (in order to obtain the ROIs), to AR-based classification of subjects into two categories: CTRL (0) and AD (1) classes. Fig. 1 shows a block diagram of the proposed system that consists of four stages: (i) masking procedure, (ii) discretization of mean intensity for feature selection, (iii) AR mining, (iv) leave-one-out (loo) cross-validation (CV).

5.1. Masking

First of all, the histogram is calculated over a mean control image to segment it into  $K_1$  subimages that consist of the voxels whose intensities belong to each bin. This is also called image thresholding as it is based on the assumption that objects can be distinguished by their intensity level (Nakib, Oulhadj, & Siarry, 2007). The mask discards the voxels of the subimage with a value of zero (represented in blue in Fig. 2).

Fig. 2 depicts (in the first row for SPECT and in the second one for PET) the transaxial slice masks obtained from the average of control images which are represented in Fig. 2a and g respectively for both databases when the  $K_1 = 5$  subimages (from 1 to 5 in Fig. 2b–f and h–l) are segmented by means of an intensity histo-

gram. It is observed that the selected masks (the 4th for SPECT depicted in Fig. 2e and the 5th for PET in Fig. 2l) include the most relevant voxels for the AD diagnosis since they are situated in the temporoparietal regions.

5.2. Voxels selected by discretization

The mask coordinates are the center of the 3D  $v \times v \times v$ -sized cubic blocks. Each block is represented by a continuous feature that consists of the mean intensity ( $I_{mean}$ ) of the voxels whose intensity belongs to the mask range  $[I_{min}, I_{max}]$ . The discretization consists of an equal-width-size histogram applied to the range  $[I_{mean-min}, I_{mean-max}]$  dividing it into  $K_2$  bins of equal width. Discretized bins are used independently or in a combined way to define the intervals of selected ROI value for each subject. These ROIs act as inputs for the AR-mining algorithm (named Apriori). It is demonstrated that while lower discretized bin combinations use to be noisy for classification, higher ones are likely to show relevant information for the AD early detection (see Tables 3 and 4).

5.3. AR mining and classification

In the training stage, AR mining captures co-occurrence patterns (Jukic & Nestorov, 2006) within data of controls. Generally speaking, control patterns are less variable than AD patterns thus

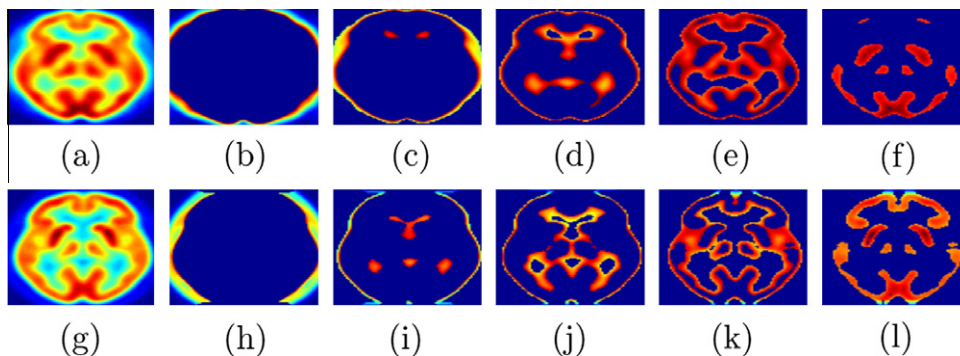


Fig. 2. Transaxial slice of the image histogram segmentation (SPECT in the first row and PET in the second one) obtained from SPECT average images (depicted in (a) and (g)) which are respectively divided in the following  $K_1 = 5$  subimages corresponding to each bin.

**Table 3**

Accuracy rate (%) taking 4th bin subimage ( $K_1 = 5$ ) as mask and combining different bins of discretization stage ( $K_2 = 5$ ) for SPECT database. Bold values show the highest accuracy rates.

Bins of discretization	1	2	3	4	5
1	–	44.33	64.95	<b>96.91</b>	<b>96.91</b>
2	44.33	44.33	64.95	51.55	<b>96.91</b>
3	64.95	64.95	79.38	74.23	67.01
4	<b>96.91</b>	51.55	74.23	<b>96.91</b>	95.88
5	<b>96.91</b>	<b>96.91</b>	67.01	95.88	<b>96.91</b>

**Table 4**

Accuracy rate (%) taking 5th bin subimage ( $K_1 = 5$ ) as mask and combining different bins of discretization stage ( $K_2 = 5$ ) for PET database. Bold values show the highest accuracy rates.

Bins of discretization	1	2	3	4	5
1	–	–	86.67	91.33	78
2	–	–	86.67	57.33	78
3	86.67	86.67	88	64	59.33
4	<b>91.33</b>	57.33	64	<b>91.33</b>	<b>92</b>
5	78	78	59.33	<b>92</b>	78

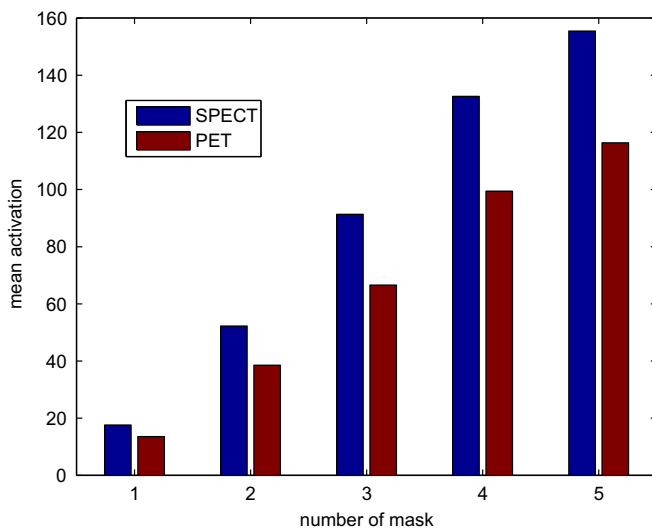


**Fig. 3.** Average of 3D features centered in mask coordinates with values the mean activation for SPECT and PET databases.

they are more suitable for obtaining relevant relationships among brain regions using ARs, which will not be satisfied by AD patients. A rule in this context is the relationship among transaction items with enough support and confidence, as they are identified with discriminant regions in the brain for the early AD diagnosis. The AR mining process employs Apriori algorithm for finding sets of items with confidence and support greater than a minimum support (called *minsupp*) and minimum confidence (called *minconf*) (often called frequent itemsets) established by the user. In this work, *minsupp* and *minconf* are selected the maxima, that is, 100%. This guarantees that the number of rules obtained is reduced and that only the most distinguishing features for the classification stage are used. In addition, at 100% of *minconf* and *minsupp*, it is emphasized that all controls are correctly classified obtaining specificities of 100%. For the lowest bins, the ROIs are worse associated and the ARs at the highest *minsupp* and *minconf* may not exist (see Tables 3 and 4).

The AR-mining process does not consider the control who is being evaluated in the test phase, avoiding in this way the over-training in an iterative loop. In the test stage, following this loop

methodology, we find out for each subject the number of verified ARs. If a subject verifies more or an equal number of ARs than a class-threshold then, it is classified as CTRL otherwise as AD. Since ARs are mined from controls, it is expected that healthy subjects verify a higher number of ARs than the one verified by AD patients. As 100% *minconf* and *minsupp* are used, the maxima accuracy rates are obtained when the 100% of rules are verified (Chaves et al., 2011).

## 6. Experimental results

Several experiments were conducted in order to test the reliability of the proposed CAD system whose performance is evaluated by means of its Accuracy (Acc), Sensitivity (Sen) and Specificity (Spe).

3D-Blocks of  $9 \times 9 \times 9$ -size centered in mask coordinates were selected and discretization procedure for ROI selection is carried out. The center coordinates of the 3D blocks are restricted to be in  $4 \times 4 \times 4$  3D grid. Both masking and discretization are performed with  $K_1, K_2 = 5$ .

As masking is concerned, the histogram shows an equal-width distribution covering  $K_1$  ranges. If too few or too many ranges are used, the histogram can be misleading. Selected  $K_1 = 5$  is intended to show this trade-off in the light of the results with both databases.

Related to discretization,  $K_2 = 5$  was selected as a trade-off between computational cost and accuracy results: if  $K_2$  increases, the number of selected ROIs by discretization decreases, accelerating in this way the AR-mining process but discarding important regions for the AD early diagnosis. On the other hand, as  $K_2$  decreases, computational cost slows down and does not improve classification rates in this case.

It is remarkable that the quality of the ARs for classification is better when *minsupp* and *minconf* are selected of 100% as the control pattern is distinguished better from the AD pattern. At this value, when selected discretized bins (usually lower ones) have not predictive power enough, no ARs are extracted (see this effect in Tables 3 and 4 for discretized bins 1 and 2).

### 6.1. Experiments with SPECT database

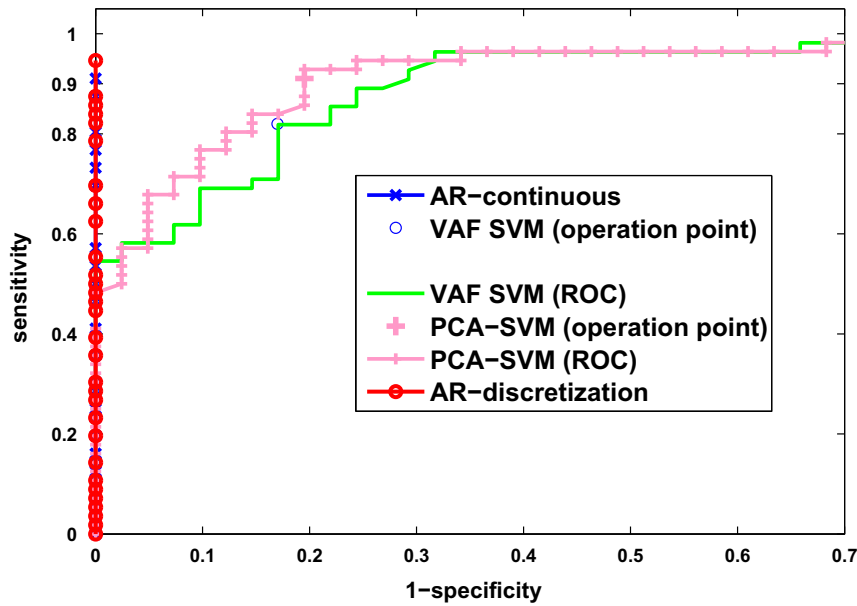
In the masking process, the fourth segmented subimage (see Fig. 2e) from  $K_1 = 5$  is selected as it provides the best classification results.

Table 3 shows the discretized bin combinations when  $K_2 = 5$  and it is demonstrated that when the higher bins are included in the combination, accuracy results are likely to improve. In fact, when the 5th discretized bin is combined with the 1st, 2nd or 5th, 96.91% of accuracy is obtained (94.64% sensitivity and 100% specificity), outperforming the continuous AR-based technique Chaves et al. (2011) with results ( $Acc = 94.87\%$ ,  $Sen = 91.07\%$ ,  $Spe = 100\%$ ).

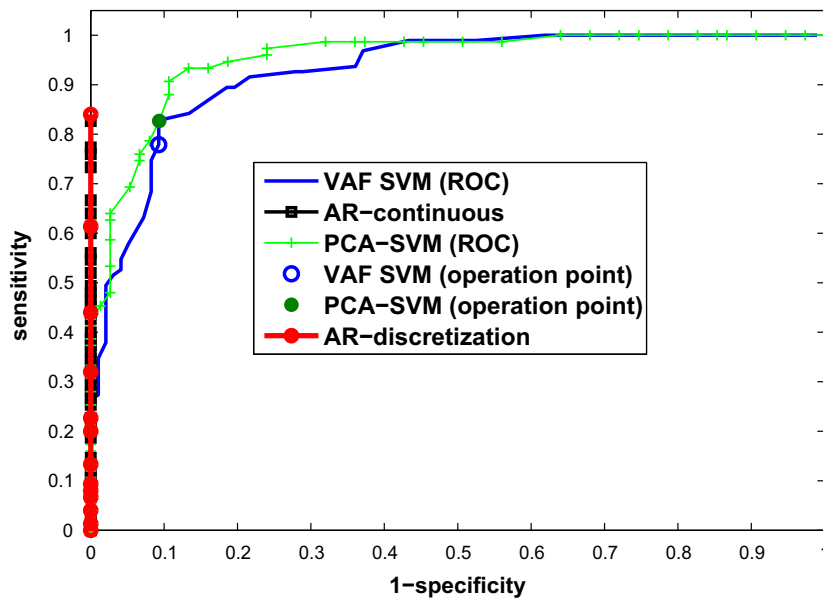
### 6.2. Experiments with PET database

Generally speaking, PET is less activated than SPECT. This is demonstrated in Fig. 3 that shows the average of mean intensity features (3D blocks  $9 \times 9 \times 9$  sized with center in mask coordinates) for PET and SPECT databases. It is remarkable that the used 4th mask in SPECT and the 5th one in PET have the most similar average of mean intensity value (115.38 for SPECT and 132.59 for PET) in comparison with the remaining subimages, guaranteeing in this way better detection ability.

Table 4 shows discretized bin combinations for PET when the mask presented in Fig. 2l is applied, reaching rates of  $Acc = 92\%$ ,  $Sen = 84\%$  and  $Spe = 100\%$  (when the 4th and the 5th bins are com-



(a)



(b)

**Fig. 4.** ROC Curve (a) SPECT and (b) PET databases for the proposed method when the best discretized bins are combined. Comparison with AR-baseline for continuous features and other reported methods: VAF-SVM and PCA-SVM.

bined) outperforming the AR-based continuous case ( $Acc = 91.33\%$ ,  $Sen = 82.6\%$ ,  $Spe = 100\%$ ) Chaves, Ramírez, Górriz, and Illn (2012). As for the SPECT database, the best results were obtained for the higher discretized bins as they show more activation and better detection ability for the AD.

6.3. ROC study

The receiver operating characteristic (ROC) curve has been demonstrated to be very effective for the evaluation of CAD systems. These plots show the trade-off between the specificity and sensitivity of the CAD system as the detection threshold varies.

Fig. 4 shows the ROC curves of the discretized-AR-based CAD system for SPECT (Fig. 4a) and PET (Fig. 4b). ROC curve for the proposed method is depicted at the best results of the discretized bin combinations (reported in Sections 6.1 and 6.2). As shifted up and to the left, this work outperforms other reported techniques such as voxels as features (VAF), principal component analysis (PCA) in combination with support vector machine (SVM) López et al. (2009), Angulo, Anguita, Gonzalez-Abril, and Ortega (2008), It;br/>López et al. (2011) or the AR-continuous based method (Chaves et al., 2011).

Note that, as the minconf and minsupp are selected at the maximum 100% (for continuous and discretized AR-based methods), consequently all controls are correctly classified ( $Spe = 1$  in the

ROC space) since the ARs obtained are the most discriminant in order to distinguish better normal from AD pattern.

## 7. Conclusion and outlook

Integration of discretization for feature selection and AR for classification is proposed as an effective technique in order to design a CAD system for the early diagnosis of AD. Firstly, an image histogram segmentation is applied over the mean control image in order to obtain the best mask, corresponding to higher bins (in particular the 4th for SPECT and the 5th for PET, from a total of  $K_1$  subimages). The selection of  $K_1 = 5$  for the mask obtaining implies a generalization in both databases and the assumption that the segmentation-based histogram is not misleading (which frequently occurs when too few or too many ranges are used). Secondly, an equal-width sized discretization is performed by the combination of different bins being the most activated (or higher) ones (from the total of  $K_2$ ) usually the most suitable in order to choose the relevant 3D ROIs used as input in the AR mining.  $K_2 = 5$  is selected as a trade-off between computational cost and accuracy results. The proposed method reaches  $Acc = 96.91\%$  (for SPECT) and  $92\%$  (for PET) outperforming the AR-continuous baseline method described in Chaves et al. (2011) and other reported methods such as VAF-SVM or PCA-SVM. We have shown classification results when used relevant discretized bins for AR-mining, with minsupp and minconf of 100%. In that case, at the 100% of verified rules the maxima classification results are obtained and all controls are correctly classified, that is  $Spe = 100\%$ . To sum up, the AR discovery among discrete ROIs obtained from functional images can simplify the process of learning improving the generalization of the learned results for the early diagnosis of AD.

## Acknowledgments

This work was partly supported by the MICINN of Spain under the TEC2008-02113 and TEC2012-34306 projects and the Consejería de Innovación, Ciencia y Empresa (Junta de Andalucía, Spain) under the Excellence Projects P07-TIC-02566, P09-TIC- 4530 and P11-TIC-7103. We are grateful to M. Gómez-Río and coworkers from the ‘Virgen de las Nieves’ hospital in Granada (Spain) for providing and labeling the SPECT images used in this work. The PET Data collection and sharing for this project was funded by the Alzheimer’s Disease Neuroimaging Initiative (ADNI) (National Institutes of Health Grant U01 AG024904). ADNI is funded by the National Institute on Aging, the National Institute of Biomedical Imaging and Bioengineering, and through generous contributions from the following: Abbott; Alzheimer’s Association; Alzheimer’s Drug Discovery Foundation; Amorfix Life Sciences Ltd.; AstraZeneca; Bayer HealthCare; BioClinica, Inc.; Biogen Idec Inc.; Bristol-Myers Squibb Company; Eisai Inc.; Elan Pharmaceuticals Inc.; Eli Lilly and Company; F. Hoffmann-La Roche Ltd and its affiliated company Genentech, Inc.; GE Healthcare; Innogenetics, N.V.; IXICO Ltd.; Janssen Alzheimer Immunotherapy Research & Development, LLC.; Johnson & Johnson Pharmaceutical Research & Development LLC.; Medpace, Inc.; Merck & Co., Inc.; Meso Scale Diagnostics, LLC.; Novartis Pharmaceuticals Corporation; Pfizer Inc.; Servier; Synarc Inc.; and Takeda Pharmaceutical Company. The Canadian Institutes of Health Research is providing funds to support ADNI clinical sites in Canada. Private sector contributions are facilitated by the Foundation for the National Institutes of Health (www.fnih.org). The grantee organization is the Northern California Institute for Research and Education, and the study is coordinated by the Alzheimer’s Disease Cooperative Study at the University of California, San Diego. ADNI data are disseminated by the Laboratory for Neuro Imaging at the University of California, Los Angeles. This re-

search was also supported by NIH grants P30 AG010129 and K01 AG030514.

## References

- Agrawal, R., Srikant, R. (1994). Fast Algorithms for mining association rules. In *International conference on VLDB, Santiago de Chile, Chile* (pp. 487–499).
- Angulo, C., Anguita, D., Gonzalez-Abriel, L., & Ortega, J. A. (2008). Support vector machines for interval discriminant analysis. *Neurocomputing*, 71(7/9), 1220–1229.
- Ashburner, J., & Friston, K. J. (1999). Nonlinear spatial normalization using basis functions. *Human Brain Mapping*, 7(4), 254–266.
- Brookmeyer, Ron, Johnson, Elizabeth, Ziegler-Graham, Kathryn, & Michael Arrighi, H. (2007). Forecasting the global burden of Alzheimer’s disease. *Alzheimer’s and Dementia*, 3(3), 186–191. ISSN 1552-5260, 10.1016/j.jalz.2007.04.381.
- Chaves, R., Górriz, J. M., Ramírez, J., Illán, I. A., Salas-González, D., & Gómez-Río, M. (2011). Efficient Mining of Association Rules for the Early Diagnosis of Alzheimer’s Disease. *Physics in Medicine and Biology*, 56(18), 6047–6063.
- Chaves, R., Ramírez, J., Górriz, J. M., & Illán, I. A. (2012). Functional brain image classification using association rules defined over discriminant regions. *Pattern Recognition Letters*, 33(12), 1666–1672.
- Chaves, R., Ramírez, J., Górriz, J. M., López, M., Salas-Gonzalez, D., Álvarez, I., et al. (2009). SVM-based computer-aided diagnosis of the Alzheimer’s disease using t-test NMSE feature selection with feature correlation weighting. *Neuroscience Letters*, 461(3), 293–297.
- Chaves, R., Ramírez, J., Górriz, J. M., & Puntonet, C. G. (2012). Association rule-based feature selection method for Alzheimers disease diagnosis. *Expert Systems with Applications*, 39(14), 11766–11774.
- Chmielewski, M.R., Grzymala-Busse, J.W., 1994. Global discretization of continuous attributes as preprocessing for machine learning. In *Third international workshop on rough sets and soft computing* (pp. 294–301).
- Chyzyk, D., Graña, M., Savio, A., & Maiora, J. (2012). Hybrid dendritic computing with kernel-LICA applied to Alzheimer’s disease detection in MRI Original Research Article. *Neurocomputing*, 75(1), 72–77.
- Dasseni, E., Vergyios, V. S., Elmagarmid, A. K., & Bertino, E. (2001). Hiding association rules by using confidence and support. *Lecture Notes in Computer Science*, 2137, 369–383.
- Dougherty, J., Kohavi, R., Mehran Sahami (1995). Supervised and unsupervised discretization of continuous features. In *Machine learning: proceedings on the twelfth international conference* (pp. 194–202).
- Dua, S., Singh, H., & Thompson, H. W. (2009). Associative classification of mammograms using weighted rules. *Expert Systems with Applications*, 36, 9250–9259.
- Dubois, B., Feldman, H. H., Jacova, C., DeKosky, S. T., Barberger-Gateau, P., Cummings, J., et al. (2007). Research criteria for the diagnosis of Alzheimer’s disease: revising the NINCDS ADRDA criteria. *The Lancet Neurology*, 6(8), 734–746.
- Fayyad, U.M., Irani, K.B., 1993. Multi-interval discretization of continuous valued attributes for classification learning. In *Proceedings of the 13th international joint conference on artificial intelligence* (pp. 1022–1027).
- Friston, K. J., Ashburner, J., Kiebel, S. J., Nichols, T. E., & Penny, W. D. (2007a). *Statistical Parametric Mapping: The Analysis of Functional Brain Images*. Academic Press.
- Friston, K., Ashburner, J., Kiebel, S., Nichols, T., & Penny, W. (2007b). *Statistical Parametric Mapping: The Analysis of Functional Brain Images*. Academic Press.
- He, Ruhun, Xiong, Naixue, Yang, Laurence T., & Park, Jong Hyuk (2011). Using Multi-Modal Semantic Association Rules to fuse keywords and visual features automatically for Web image retrieval. *Informative Fusion*, 12, 223–230.
- Illán, I. A., Górriz, J. M., López, M. M., Ramírez, J., Gonzalez, D. S., Segovia, F., et al. (2011). Computer aided diagnosis of Alzheimers disease using component based SVM. *Applied Soft Computing*, 11, 2376–2382.
- Jobst, K. A., Barnetson, L. P., & Shepstone, B. J. (1998). Accurate prediction of histologically confirmed alzheimer’s disease and the differential diagnosis of dementia: the use of NINCDS-ADRDA and DSM-III-R criteria, SPECT, X-ray CT, and apo e4 in medial temporal lobe dementias, Oxford project to investigate memory and aging. *International Psychogeriatrics*, 10(3), 271–302.
- Jukic, N., & Nestorov, S. (2006). Comprehensive data warehouse exploration with qualified association-rule mining. *Decision Support Systems*, 42, 859–878.
- Kabir, M., Islam, M., & Murase, K. (2010). A new wrapper feature selection approach using neural network. *Original Research Article Neurocomputing*, 73(16:18), 3273–3283.
- Kim, Kyoung-Jae, & Han, Ingoo (2000). Genetic algorithms approach to feature discretization in artificial neural networks for the prediction of stock price index. *Expert Systems with Applications*, 19(2), 125–132.
- Kogure, D., Matsuda, H., Ohnishi, T., Asada, T., Uno, M., Kunihiro, T., et al. (2000). Longitudinal evaluation of early Alzheimer disease using brain perfusion SPECT. *The Journal of Nuclear Medicine*, 41(7), 1155–1162.
- Kotsiantis, S., & Kanellopoulos, D. (2006). Discretization Techniques: A recent survey. *GESTS International Transactions on Computer Science and Engineering*, 32(1), 47–58.
- Liu, B., Hsu, W., & Ma, Y. (1998). Integrating classification and association rule mining. *Knowledge Discovery and Data Mining*, 80–86.
- López, M., Ramírez, J., Górriz, J. M., Álvarez, I., Salas-Gonzalez, D., Segovia, F., et al. (2011). The Alzheimer’s Disease Neuroimaging Initiative, Principal component analysis-based techniques and supervised classification schemes for the early detection of Alzheimer’s disease. *Neurocomputing*, 74(8), 1260–1271.

- López, M., Ramírez, J., Górriz, J. M., Salas-Gonzalez, D., Álvarez, I., Segovia, F., et al. (2009). Automatic tool for the Alzheimer's disease diagnosis using PCA and bayesian classification rules. *IET Electronics Letters*, 45(8), 389–391.
- Martínez-Murcia, F. J., Górriz, J. M., Ramírez b, J., Puntonet, C. G., & Salas-Gonzalez, D. (2012). for the Alzheimer's Disease Neuroimaging Initiative. *Computer Aided Diagnosis tool for Alzheimer's Disease based on Mann-Whitney-Wilcoxon U-Test Expert Systems with Applications*, 39(10), 9676–9685.
- Nakib, A., Oulhadj, H., & Siarry, P. (2007). Image histogram thresholding based on multiobjective optimization. *Signal Processing*, 87, 25162534.
- Ng, S., Villemagne, V. L., Berlangieri, S., et al. (2007). Visual assessment versus quantitative assessment of 11c-PiB PET and 18f-FDG PET for detection of alzheimer's disease. *J. Nucl. Med.*, 48, 547–552.
- Park, Cheong Hee, & Lee, Moonhwi (2009). A SVM-based discretization method with application to associative classification. *Expert Systems with Applications*, 36(3), 4784–4787.
- Ribeiro, M. X., Bugatti, P. H., Traina, C., Marques, P. M. A., Rosa, N. A., & Traina, A. J. M. (2009). Supporting content-based image retrieval and computer-aided diagnosis systems with association rule-based techniques. *Data and Knowledge Engineering*, 68, 1370–1382.
- Ribeiro, M. X., Traina, A. J. M., Traina, C., Jr., & Azevedo-Marques, P. M. (2008). An association rule-based method to support medical image diagnosis with efficiency. *IEEE Transactions on Multimedia*, 2(10), 277–285.
- Salas-Gonzalez, D., Górriz, J. M., Ramírez, J., Lassl, A., & Puntonet, C. G. (2008). Improved gauss-newton optimization methods in affine registration of SPECT brain images. *IET Electronics Letters*, 44(22), 1291–1292.
- Segovia, F., Górriz, J. M., Ramírez, J., Salas-Gonzalez, D., Álvarez, I., López, M., et al. (2012). A comparative study of feature extraction methods for the diagnosis of Alzheimer's disease using the ADNI database Original Research Article. *Neurocomputing*, 75(1), 64–71.